Magnetic-Based Motion Control of a Helical Robot using Two Synchronized Rotating Dipole Fields

Mahmoud E. Alshafeei*, Abdelrahman Hosney*, Anke Klingner*, Sarthak Misra† and Islam S. M. Khalil*

Abstract— This work addresses the magnetic-based control of a helical robot and the mitigation of the magnetic forces on its dipole moment during radial steering using rotating permanent magnets. A magnetic system with two synchronized permanent magnets that rotate quasistatically is used to move the helical robot (length and diameter of 12.5 mm and 4 mm, respectively). We experimentally demonstrate that using two synchronized permanent magnets for radial steering of a helical robot achieves higher motion stability, as opposed to propulsion using single rotating dipole field. The two synchronized dipole fields decrease the lateral oscillation (average peak-to-peak amplitude) of the helical robot by 37%, compared to the radial steering using a single dipole field at angular velocity of 31 rad/s. We also show that driving the helical robot using two synchronized rotating magnets achieves average swimming speed of 2.1 mm/s, whereas the single rotating dipole field achieves average swimming speed of 0.4 mm/s at angular velocity of 31 rad/s for the rotating permanent magnets. The proposed configuration of the helical propulsion allows us to decrease the magnetic forces that could cause tissue damage or potential trauma for *in vivo* applications.

I. INTRODUCTION

Driving helical magnetic robots (in microscale [1], [2] and mesoscale [3], [4]) using rotating permanent magnets has the potential to make them viable for clinical applications [5], [6], [7], [8]. The magnetic torque exerted on their dipole moment allows them to rotate, and hence move through rolling, swimming, crawling or through screw-based motion in tissue [9]. However, for *in vivo* applications, the attractive magnetic forces that are generated during radial steering [10] of a helical robot must be managed or completely eliminated to accomplish safe interaction between the helical robots and the surrounding tissue.

Mahoney *et al.* have demonstrated that the attractive forces acting on a magnetic microrobot can be converted into a lateral force by rotating the actuator dipole according to an open-loop trajectory [11]. This conversion allows for reducing the attractive component, assisting the rolling of microrobots, and overcoming gravitational forces. Abbott *et al.* have shown that pure torque can be applied on a soft-magnetic body using magnetic fields of two dipole pair configurations [12]. The axial and radial control of a helical robot have been presented by Fountain *et al.* [10]. It has also

(a) 0° with respect to y-axis (b) 45° with respect to y-axis

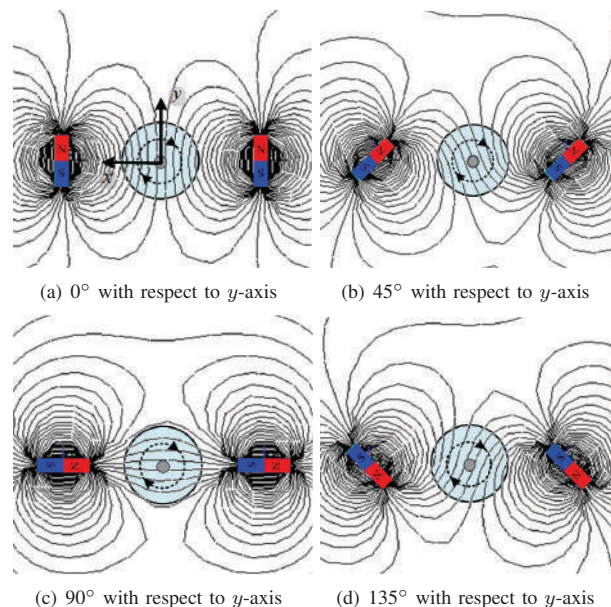(c) 90° with respect to y-axis (d) 135° with respect to y-axis

Fig. 1. Four representative orientations of two synchronized rotating dipole fields that are used to propel a helical robot (small gray circle) in a glass tube (light turquoise circle). Simulation of the magnetic fields is done using ANSYS (ANSYS Mechanical APDL 15.0, ANSYS, Pennsylvania, USA). (a) The permanent magnets have 0° with respect to y-axis. (b) The permanent magnets have 45° with respect to y-axis. (c) The permanent magnets have 90° with respect to y-axis. (d) The permanent magnets have 135° with respect to y-axis.

been shown that the radial control is more complicated than the axial control due to the variations in the magnetic field and gradients throughout the rotation of the dipole field.

In this study, we experimentally demonstrate that the attractive forces exerted on the helical robots can be mitigated using two synchronized rotating permanent magnets (Fig. 1). A magnetic-based robotic system is developed to allow for the motion control of the helical robot inside glass tubes with two diameters (approximately twice and 10 times larger than the diameter of the helical robot). The configuration of the magnetic-based robotic system and the synchronized rotating permanent magnets allow the helical robot to rotate and swim while eliminating the attractive forces that act in opposite directions on its dipole. We compare the average peak-to-peak amplitude of the oscillation and the average swimming speed of the helical robot during propulsion using two synchronized rotating dipole fields and a single rotating dipole field. This comparison allows us to study the effect of

the two synchronized dipole fields on the helical propulsion of the robot.

The remainder of this paper is organized as follows: Section II provides analysis pertaining to the governing equations of motion of a helical robot and the strategy used to mitigate the attractive forces. Section III provides descriptions of the magnetic-based robotic system. In addition, the magnetic-based motion control results are included for two cases. The first case is done using a single rotating dipole field, whereas the second case is done using two synchronized rotating dipole fields. Section IV provides a discussion pertaining to the effect of the diameter of the containing tube on the motion stability of the helical robot. Finally, Section V concludes and provides directions for future work.

II. MITIGATION OF THE ATTRACTIVE MAGNETIC FORCES ON HELICAL ROBOTS

The helical robot (Fig. 2) has a similar propulsion mechanism to that of the *E. Coli*. It generates a driving force when its helical structure is rotated inside a fluid. The helical robot is contained inside tubes with inner diameters of 10 mm and 40 mm. It is made of a helical spring with diameter of 4 mm and length of 12.5 mm. The number of turns and the wire diameter are 4 turns and 0.7 mm, respectively. A cylindrical NdFeB magnet is attached to the head of the spring with a dipole polarity perpendicular to the helical robot longtidunal axis. Under the influence of a magnetic field, the magnetic force $\left(\mathbf{F}(\mathbf{P}) \in \mathbb{R}^{3 \times 1}\right)$ and torque $\left(\mathbf{T}(\mathbf{P}) \in \mathbb{R}^{3 \times 1}\right)$ experienced by a helical robot located at position $\left(\mathbf{P} \in \mathbb{R}^{3 \times 1}\right)$ are given by [13], [14], [15]

$$\mathbf{F}(\mathbf{P}) = (\mathbf{m} \cdot \nabla)\mathbf{B}(\mathbf{P}) \quad \text{and} \quad \mathbf{T}(\mathbf{P}) = \mathbf{m} \times \mathbf{B}(\mathbf{P}), \quad (1)$$

where $\mathbf{m} \in \mathbb{R}^{3 \times 1}$ and $\mathbf{B}(\mathbf{P}) \in \mathbb{R}^{3 \times 1}$ are the magnetic dipole moment of the helical robot and the induced magnetic field, respectively.

A. Propulsion using Single Dipole Field

Using a single magnetic dipole field, the magnetic force exerted on the magnetic dipole of the helical robot is given by [16]

$$\begin{bmatrix} F_x(\mathbf{P}) & F_y(\mathbf{P}) & F_z(\mathbf{P}) \end{bmatrix}^{\mathrm{T}} = (\mathbf{m} \cdot \nabla)\mathbf{B}(\mathbf{P}), \quad (2)$$

where $F_i(\mathbf{P})$ is the magnetic force component along the ith axis for $(i = x, y, z)$. Further, ∇ is the gradient operator and is given by

$$\nabla = \begin{bmatrix} \frac{\partial}{\partial x} & \frac{\partial}{\partial y} & \frac{\partial}{\partial z} \end{bmatrix}^{\mathrm{T}}. \quad (3)$$

In the configuration shown in Fig. 1(a), the gradients $\partial \mathbf{B}(\mathbf{P})/\partial x$, $\partial \mathbf{B}(\mathbf{P})/\partial y$, and $\partial \mathbf{B}(\mathbf{P})/\partial z$ are not zero. Therefore, the magnetic forces along x- and y-axis pull the helical robots towards the inner wall of the tube, whereas the magnetic force component along z-axis could contribute to the propulsive force of the helical robot.
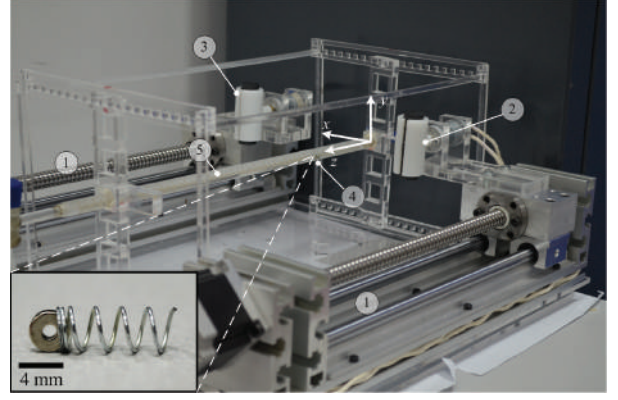

Fig. 2. A magnetic-based robotic system for the motion control of a helical robot (inset). The system consists of two synchronized linear motion stages ①. Each stage holds a rotating permanent magnet (② and ③) to actuate the helical robot ④. The rotating permanent magnets are also synchronized using a control system. The helical robot is contained inside a glass tube ⑤ with inner diameter of 10 mm. The synchronized rotation of the rotating permanent magnets allows us to eliminate the attractive components of the magnetic force on the magnetic dipole of the helical robot. The diameter, length and wire diameter of the helical robot are 4 mm, 12.5 mm, and 0.7 mm, respectively.

B. Propulsion using Two Synchronized Dipole Fields

Pure magnetic torque on the magnetic dipole of the helical robot can be accomplished based on the following equality [12]

$$\partial \mathbf{B}(\mathbf{P})/\partial x = \partial \mathbf{B}(\mathbf{P})/\partial y = \partial \mathbf{B}(\mathbf{P})/\partial z = 0. \quad (4)$$

Equation (4) can be accomplished at a point $(\mathbf{P})$ using the configuration shown in Fig. 1. In this configuration, two rotating dipole fields are mounted in opposite sides of the glass tube, and are synchronized using a motion control system. The pure torque point of this configuration has to coincide with the axis of the helical robot to eliminate the magnetic forces on its dipole. In this case, the rotational dynamics of the helical robot is given by

$$\mid \mathbf{B}(\mathbf{P}) \mid\mid \mathbf{m} \mid \sin \theta + \alpha \omega = 0, \quad (5)$$

where θ and ω are the angle between the induced magnetic field and the magnetic dipole moment of the helical robot, and the angular velocity of the helical robot (with respect to its longitudinal axis), respectively. Further, α is the rotational drag coefficient that depends on the shape of the helical robot and the viscosity of the fluid. The first term in (5) allows the helical robot to rotate and generate a thrust force [19]. The linear dynamics of the helical robot is given by

$$f + F_z(\mathbf{P}) + F_{\mathrm{d}}(\dot{\mathbf{P}}) = 0, \quad (6)$$

where f and $F_{\mathrm{d}}(\dot{\mathbf{P}})$ are the thrust force due to the helical propulsion and the drag force, respectively. Further, $\dot{\mathbf{P}}$ is the velocity of the helical robot. In (6), the direction of rotation is controlled based on the direction of rotation of the rotating permanent magnets. This allows us to achieve forward and backward propulsion of the helical robot. The magnetic configurations shown in Fig. 1 is implemented using a magnetic-based robotic system.
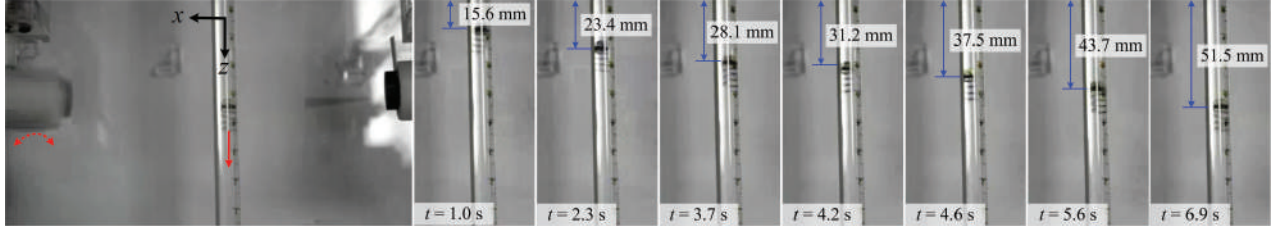
Fig. 3. A representative open-loop motion control experiment of a helical robot using a single rotating dipole field. The helical robot swims under the influence of the rotating magnetic fields, and exhibits undesirable lateral oscillations due to the attractive magnetic forces exerted on its magnetic dipole. The angular velocity of the rotating permanent magnet is 31 rad/s, and the linear speed of the helical robot is 0.5 mm/s. The red arrow indicates direction of motion of the helical robot, whereas the dashed red arrow indicates the rotation of the single dipole field. *Please refer to the accompanying video that demonstrates the motion of the helical robot using single rotating dipole field inside a glass tube with inner diameter of 10 mm.*
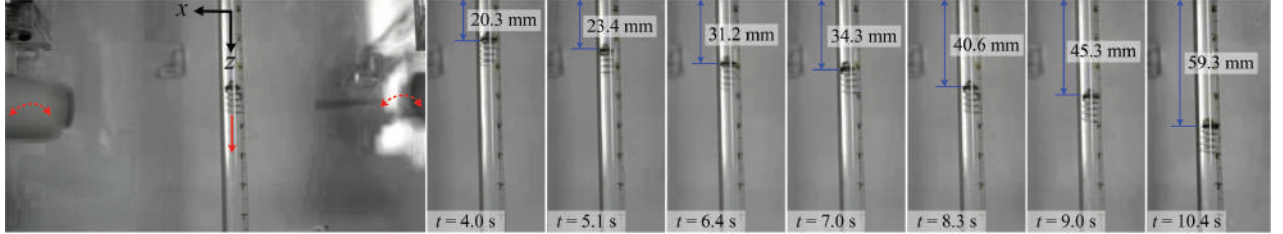

Fig. 4. A representative open-loop motion control experiment of a helical robot using two synchronized rotating dipole fields. The helical robot swims under the influence of the rotating magnetic fields, and exhibits less lateral oscillations compared to propulsion using single rotating dipole field. The angular velocity of the rotating permanent magnet is 31 rad/s, and the linear speed of the helical robot is 2.1 mm/s. The red arrow indicates direction of motion of the helical robot, whereas the dashed read arrows indicate the rotating permanent magnets. *Please refer to the accompanying video that demonstrates the motion of the helical robot using two synchronized rotating dipole fields inside a glass tube with inner diameter of 10 mm.*

C. Magnetic-Based Robotic System

We devise a magnetic-based robotic system to achieve pure torque that allows us to eliminate the attractive components of the magnetic force on the helical robot. This system consists of two synchronized linear motion stages, two rotating permanent magnets, and a glass tube that contains the helical robot inside water. The travel of the motion stage is 300 mm. Motion of the linear motion stages and the rotating permanent magnets is controlled using Arduino control board (Arduino Mega 2560, Arduino, Memphis, Tennessee, USA). Position of the helical robot is detected using a feature tracking algorithm [17], [18]. We use a Ryanteck Raspberry Pi Board (RTK RPi M.C.B, Ryanteck LTD, Cambridgeshire, United Kingdom) for the image processing and the feature tracking. The distance between the tube and the motion stages is 6 cm. Permanent magnets are attached to the DC motors using plastic adapters. The DC motors provides maximum angular velocity of approximately 50 rad/s, whereas the maximum linear speed of the linear motion stages is 100 mm/s. The two motion stages are mounted parallel to each other and to the tube, as shown in Fig. 2. The configuration of the magnetic-based robotic system is designed and developed such that the distance between the rotating permanent magnets and the helical robot can be adjusted, and glass tubes with different diameters can be used to contain the helical robots. This allows us to experimentally investigate the motion stability of the helical robot under the influence of magnetic fields generated using single and two synchronized dipole fields.

III. EXPERIMENTAL RESULTS

The effect of the single and two synchronized rotating dipole fields on the motion of the helical robot is experimentally investigated. First, we control the motion of the helical robot using a single rotating dipole field. Fig. 3 provides a representative open-loop control of the helical robot using a single rotating dipole field. The angular velocity of the rotating permanent magnet is controlled to be 31 rad/s. The linear speed of the helical robot is calculated to be 0.5 mm/s. We observe that the helical robot moves using its helical propulsion and exhibits lateral oscillation due to the attractive force components. The maximum peak-to-peak amplitude of this oscillation is calculated to be 1.2 mm. Second, we control the helical robot using two synchronized dipole fields, as shown in Fig. 4. The two rotating dipole fields are synchronized using the control system to eliminate the attractive force components. The angular velocity of the rotating permanent magnets are controlled to be 31 rad/s, and the linear speed of the helical robot is calculated to be 2.1 mm/s. We observe that the undesirable oscillation is decreased. In this representative experiment, the maximum peak-to-peak amplitude of the oscillation is calculated to be 0.75 mm.

The lateral oscillation of the helical robot generated using the single and synchronized rotating dipole fields is shown in Fig. 5. This comparison shows that the maximum peak-to-peak amplitude of the two synchronized dipole fields is 37.5% less than that caused by the single rotating dipole field. This amplitude decrease indicates that using two syn-
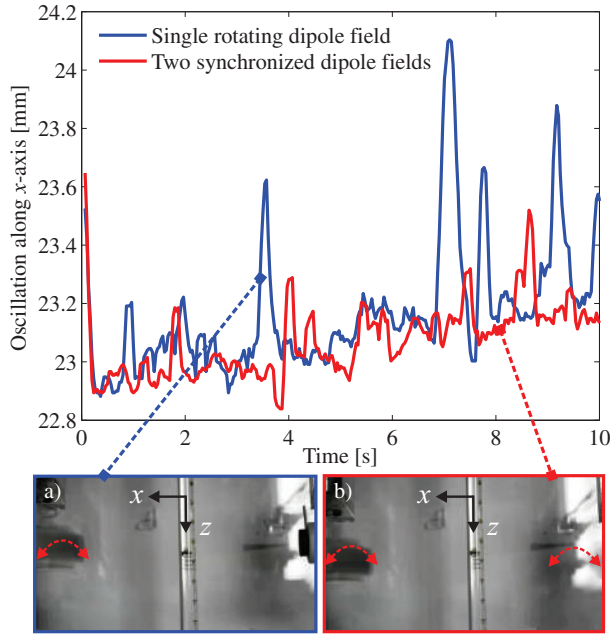
Fig. 5. Oscillation of the helical robot during swimming under the influence of the rotating magnetic fields. These fields are generated using a single dipole field (a) and two synchronized dipole fields (b). The permanent magnets are rotated at a constant angular velocity of 31 rad/s. In this representative experiment, the maximum peak-to-peak amplitudes of the helical robot oscillation are 1.2 mm and 0.75 mm for the single and synchronized dipole fields, respectively. *Please refer to the accompanying video that demonstrates the propulsion of the helical robot using single and two rotating dipole fields.*

chronized dipole fields mitigate the effect of the attractive forces on the helical robot. We repeat this trial 3 times and calculate the average peak-to-peak amplitude of the helical robot for the single and two synchronized dipole fields. The average peak-to-peak amplitudes of the helical robot oscillation are calculated to be 1.17 mm and 0.46 mm for the single and two synchronized dipole fields, respectively.

The average peak-to-peak amplitudes are calculated at 4 angular velocities (26 rad/s, 31 rad/s, 36 rad/s, and 41 rad/s) of the rotating permanent magnet. This experiment is done for the single and two synchronized rotating dipole fields. Table I provides the experimental results of this experiment. We observe that the average peak-to-peak amplitude of the synchronized rotating dipole field is 67.8%, 60.6%, 85.7%, and 87.5% less than that of the single rotating dipole field for angular velocities of 26 rad/s, 31 rad/s, 36 rad/s, and 41 rad/s, respectively.

We also investigate the effect of the synchronized rotating dipole fields on the swimming speed of the helical robot. The average swimming speeds of the helical robot are calculated for the single and synchronized rotating dipole fields. The swimming speed is calculated for a range of angular velocities of 10 rad/s to 40 rad/s for the rotating permanent magnets. Fig. 6 shows the response of the helical robot to the single and synchronized rotating dipole fields.
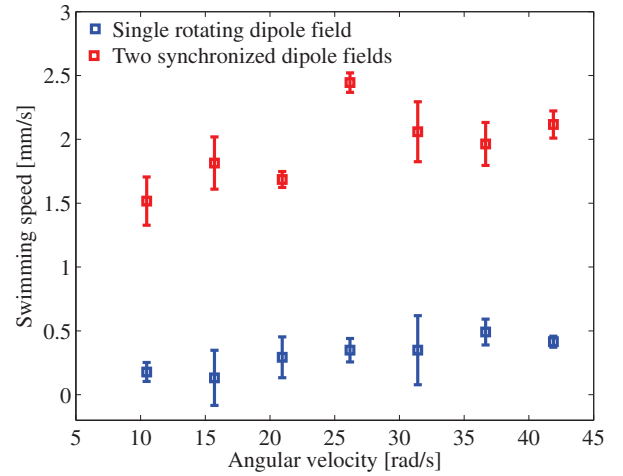

Fig. 6. Average swimming speed of the helical robot for single and two synchronized rotating dipole fields. The average swimming speeds are calculated from 3 trials at each angular velocity. The single rotating dipole field is generated using a rotating permanent magnet, whereas the opposite dipole fields are generated using two synchronized rotating permanent magnets. This experiment is done inside glass tube with inner diameter of 10 mm. Position of the helical robot is detected using a feature tracking algorithm [17], [18], and is used to calculate the swimming speed of the helical robot.

We observe that the swimming speed of the helical robot has a maximum at angular velocity of 26 rad/s, for the helical propulsion using synchronized dipole fields. However, the average swimming speed of the helical robot fluctuates as we increase the angular velocity of the single rotating dipole field.

We also observe that the maximum swimming speed accomplished using the synchronized dipole fields is greater than that of the single dipole field by 525%, at angular velocity of 26 rad/s. We attribute this increase in the swimming speed to the higher magnetic fields applied using the synchronized dipole fields. In this case the magnetic fields are superimposed, as shown in Fig. 1(b), and increase the magnetic torque exerted on magnetic dipole of the helical robot. This increase in the magnetic torque results in a greater

TABLE I

PEAK-TO-PEAK AMPLITUDES OF THE HELICAL ROBOTS UNDER THE INFLUENCE OF THE ROTATING MAGNETIC FIELDS GENERATED USING SINGLE AND SYNCHRONIZED ROTATING DIPOLE FIELDS AT 4 REPRESENTATIVE FREQUENCIES. THE AVERAGE AMPLITUDES ARE CALCULATED FROM 3 TRIALS FOR EACH FREQUENCY. THESE EXPERIMENT ARE DONE INSIDE A TUBE WITH INNER DIAMETER OF 10 MM, AND A HELICAL ROBOT WITH LENGTH AND DIAMETER OF 12.5 MM AND 4 MM, RESPECTIVELY.

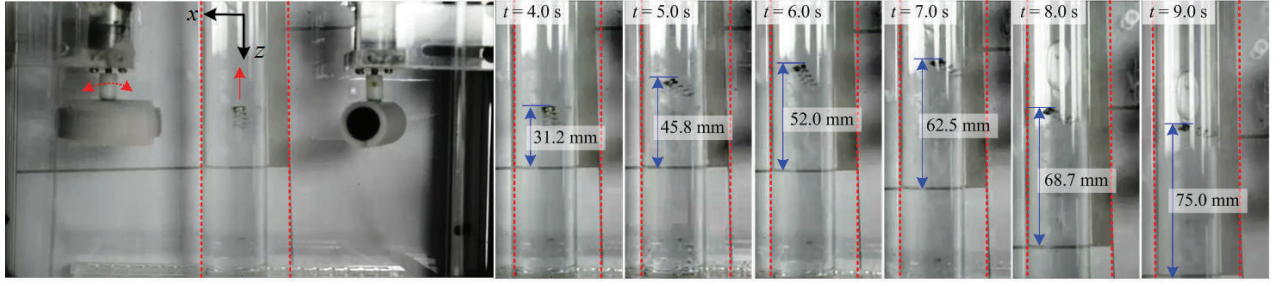| Angular velocity of magnets [rad/s]	26	31	36	41
Single dipole field [mm]	1.12	1.17	1.19	1.2
Two synchronized dipole fields [mm]	0.36	0.46	0.17	0.15

Fig. 7. A representative open-loop motion control experiment of a helical robot using a single rotating dipole field inside a glass tube with inner diameter of 3.6 cm (indicated by the dashed red lines). The helical robot swims under the influence of the rotating magnetic fields, and exhibits undesirable rotations due to the attractive magnetic forces exerted on its magnetic dipole. The helical robot exhibits lateral oscillation, random rotations, and generates enough propulsion to move away from the magnetic source. The blue arrow indicates the distance travelled by the helical robot. *Please refer to the accompanying video that demonstrates the motion of the helical robot using single rotating dipole field inside a glass tube with inner diameter of 3.6 cm.*
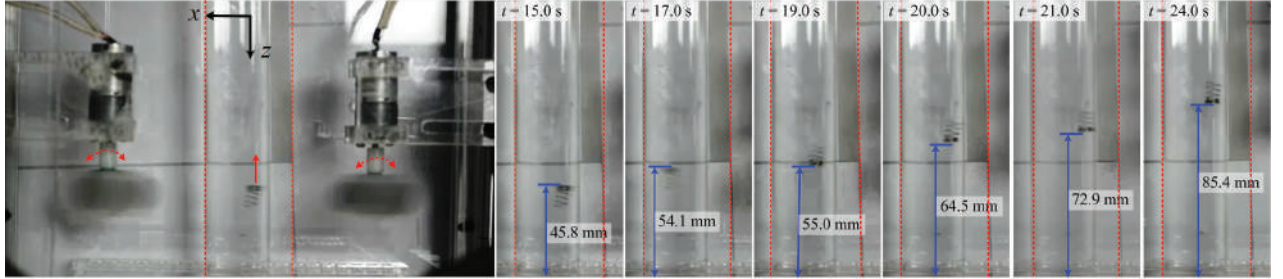

Fig. 8. A representative open-loop motion control experiment of a helical robot using two synchronized rotating dipole field inside a glass tube with inner diameter of 3.6 cm (indicated by the dashed red lines). The helical robot swims under the influence of the rotating magnetic fields, and exhibits oscillations between the dipole fields due to the to unstable equilibria [12] of the configuration. The blue arrow indicates the distance travelled by the helical robot. *Please refer to the accompanying video that demonstrates the motion of the helical robot using two synchronized rotating dipole fields inside a glass tube with inner diameter of 3.6 cm.*

angular velocity of the helical robot at each angular velocity of the rotating permanent magnets, as opposed to the single rotating dipole field.

We also attribute the higher swimming speed of the two synchronized dipole fields propulsion to the mitigation of the attractive force components. These forces attract the helical robot towards the inner wall of the tube and result in undesirable oscillation, as shown in Fig. 5. Furthermore, the attractive forces components increase the friction between the inner wall of the tube and the helical robot, and hence result in a decrease in the swimming speed during single dipole field propulsion. *Please refer to the accompanying video that demonstrates the helical propulsion inside a tube with inner diameter of 10 mm under the influence of magnetic fields generated using single and two synchronized rotating dipole fields.*

IV. DISCUSSION

The helical propulsion of helical robots is achieved usually inside tubes and lumens with inner diameters that are slightly larger than the outer diameter of the helical robots [10]. Some of our experimental results are done using glass tubes with inner diameter of 10 mm. These tubes constrain the motion of the helical robot and allow only for swimming along the longitudinal axis of the tube or the lumen. Using a single dipole field to propel the helical robot results in attractive forces that pull the helical robot towards the inner wall of the tube. On the other hand, using the synchronized dipole fields decreases these attractive forces and result in a relative increase in the swimming speed (Section III). However, the configuration of the two rotating permanent magnets provides an unstable equilibria [12]. This instability does not have much influence on the motion of the helical robot due to the constrain provided by the tube that contains the helical robot (Figs. 3 and 4).

We repeat the helical propulsion experiments inside tubes with inner diameter of 3.6 cm (approximately 10 times greater than the diameter of the helical robot) using the single and synchronized rotating dipole fields. We observe that using single dipole field the motion of the helical robot is unstable and the helical robot moves in random directions. In addition, the helical robot moves away from the magnetic source. Fig. 7 shows a representative result of the helical robot inside the large tube. Not only do we observe lateral oscillation towards the inner wall of the tube, but we also observe random rotations and the helical robot eventually produces enough propulsion force to move away from the magnetic source. At time, $t = 4$ seconds, the helical robot starts to rotate and move sideways. After time, $t = 9$ seconds the helical robot moves way from the magnetic source.

Using synchronized dipole fields we observe only lateral oscillation of the helical robot, as shown in Fig. 8.

This oscillation is due to the unstable equilibria of the configuration. At time, $t = 17$ second, the helical robot flips its direction and exhibits lateral oscillations within the walls of the tube. However, the robot does not move away from the magnetic source (the two synchronized rotating magnetic dipole), unlike the propulsion using single dipole field. Therefore, using synchronized rotating fields along with a closed-loop control based on visual feedback from the helical robot would allow us to control the motion of the helical robot inside tubes with relatively large diameters. *Please refer to the accompanying video that demonstrates the helical propulsion inside a tube with inner diameter of 3.6 cm under the influence of a single and two synchronized rotating fields.*

V. CONCLUSIONS AND FUTURE WORK

We experimentally demonstrate that the attractive components of the magnetic force can be decreased by using two synchronized rotating dipole fields. Synchronization of these fields is necessary and allows us to stabilize the helical propulsion of the helical robot inside a tube. We compare the propulsion generated using the single rotating dipole field to that generated using two synchronized dipole fields. This comparison shows that the average peak-to-peak amplitude of the propulsion generated using two synchronized dipole fields is 67.8% and 87.5% less than the average peak-to-peak amplitude of the propulsion generated using a single dipole field, at angular velocities of 26 rad/s and 41 rad/s, respectively.

As part of future work, closed-loop motion control of the helical robots will be achieved using the two synchronized rotating fields. In addition, helical robots in the microscale will be developed and controlled using two rotating dipole fields under microscopic guidance. This control will be done against the flowing streams of a fluid [20]. Furthermore, our magnetic-based robotic system will be adapted by incorporating a clinical imaging modality to provide feedback to the closed-loop control system [21], [22]. Magnetic-based motion control of helical robots in three-dimensional space will also be investigated based on the propulsion provided using the two synchronized rotating dipole fields.

VI. ACKNOWLEDGMENT

REFERENCES

[1] K. E. Peyer, L. Zhang, B. J. Nelson, "Bio-inspired magnetic swimming microrobots for biomedical applications", Nanoscale, vol. 5, no. 4, pp. 1259-1272, November 2012.

[2] D. J. Bell, S. Leutenegger, K. M. Hammar, L. X. Dong, B. J. Nelson, "Flagella-like propulsion for microrobots using a magnetic nanocoil and a rotating electromagnetic field", in *Proceedings of the IEEE International Conference on Robotics and Automation (ICRA)*, pp. 1128-1133, April 2007.

[3] A. W. Mahoney, D. L. Cowan, K. M. Miller, and J. J. Abbott, "Control of untethered magnetically actuated tools using a rotating permanent magnet in any position," in *Proceedings of the IEEE International Conference on Robotics and Automation (ICRA)*, pp. 3375-3380, Minnesota, USA, May 2012.

[4] A. W. Mahoney and J. J. Abbott, "Control of untethered magnetically actuated tools with localization uncertainty using a rotating permanent magnet," in *Proceedings of the IEEE RAS/EMBS International Conference on Biomedical Robotics and Biomechatronics (BioRob)*, pp. 1632-1637, Rome, Italy, June 2012.

[5] B. J. Nelson, I. K. Kaliakatsos, and J. J. Abbott, "Microrobots for minimally invasive medicine," *Annual Review of Biomedical Engineering*, vol. 12, pp. 55-85, April 2010.

[6] J. J. Abbott, Z. Nagy, F. Beyeler, and B. J. Nelson: Robotics in the small, part I: microbotics. *IEEE Robotics and Automation Magazine*, 14(2), 92–103 (2007).

[7] J. Wang and W. Gao, "Nano/Microscale Motors: Biomedical Opportunities and Challenges," *ACS Nano*, vol. 6, no. 7, pp. 5745-5751, July 2012.

[8] L. Dong and B. J. Nelson: Tutorial - Robotics in the small part II: nanorobotics. *IEEE Robotics and Automation Magazine*, 14(3), 111–121 (2007).

[9] K. Ishiyama, K. I. Arai, M. Sendoh, and A. Yamazaki, "Spiral-type micro-machine for medical applications," J. of Micromechatronics, vol. 2, no. 1, pp. 7786, April 2002.

[10] T. W. R. Fountain, P. V. Kailat, and J. J. Abbott, "Wireless control of magnetic helical microrobots using a rotating-permanent-magnet manipulator," in *Proceedings of the IEEE International Conference on Robotics and Automation (ICRA)*, pp. 576-581, Alaska, USA, May 2010.

[11] A. W. Mahoney and J. J. Abbott, "Managing magnetic force applied to a magnetic device by a rotating dipole field," *Applied Physics Letters*, 99, September 2011.

[12] J. J. Abbott, O. Ergeneman, M. P. Kummer, A. M. Hirt, and B. J. Nelson, "Modeling magnetic torque and force for controlled manipulation of soft-magnetic bodies," *IEEE Transactions on Robotics and Automation*, vol. 23, no. 6, pp. 1247-1252, December 2007.

[13] D. Jiles, "Introduction to magnetism and magnetic materials", Taylor & Francis, 1998.

[14] T. H. Boyer, "The force on a magnetic dipole," *American Journal of Physics*, vol. 56, no. 8, pp. 688-692, August 1988.

[15] S. S. Shevkoplyas, A. C. Siegel, R. M. Westervelt, M. G. Prentiss, and G. M. Whitesides, "The force acting on a superparamagnetic bead due to an applied magnetic field," *Lab on a Chip*, vol. 7, no. 6, pp. 1294-1302, July 2007.

[16] M. P. Kummer, J. J. Abbott, B. E. Kartochvil, R. Borer, A. Sengul, and B. J. Nelson, "OctoMag: an electromagnetic system for 5-DOF wireless micromanipulation," *IEEE Transactions on Robotics*, vol. 26, no. 6, pp. 1006-1017, December 2010.

[17] J. D. Keuning, J. de Vries, L. Abelmann, and S. Misra, "Image-based magnetic control of paramagnetic microparticles in water," in *Proceedings of the IEEE International Conference of Robotics and Systems (IROS)*, pp. 421-426, San Francisco, USA, September 2011.

[18] I. S. M. Khalil, J. D. Keuning, L. Abelmann, and S. Misra, "Wireless magnetic-based control of paramagnetic microparticles," in *Proceedings of the IEEE RAS/EMBS International Conference on Biomedical Robotics and Biomechatronics (BioRob)*, pp. 460-466, Rome, Italy, June 2012.

[19] E. M. Purcell, "Life at low reynolds number," American J. Physics, vol. 45, no. 1, pp. 3-11, 1977.

[20] I. S. M. Khalil, V. Magdanz, S. Sanchez, O. G. Schmidt, and S. Misra, "The control of self-propelled microjets inside a microchannel with time-varying flow rates," *IEEE Transactions on Robotics*, vol. 30, no. 1, pp. 49-58, February 2014.

[21] I. S. M. Khalil, P. Ferreira, R. Eleutério, C. L. de Korte, and S. Misra, "Magnetic-Based closed-loop control of paramagnetic microparticles using ultrasound feedback," in *Proceedings of the IEEE International Conference on Robotics and Automation (ICRA)*, Hong Kong, China, June 2014. *In Press*

[22] S. Martel, O. Felfoul, J.-B. Mathieu, A. Chanu, S. Tamaz, M. Mohammadi, M. Mankiewicz, and N. Tabatabaei , "MRI-based medical nanorobotic platform for the control of magnetic nanoparticles and flagellated bacteria for target interventions in human capillaries," *International Journal of Robotics Research*, vol. 28, no. 9, pp. 1169-1182, September 2009.